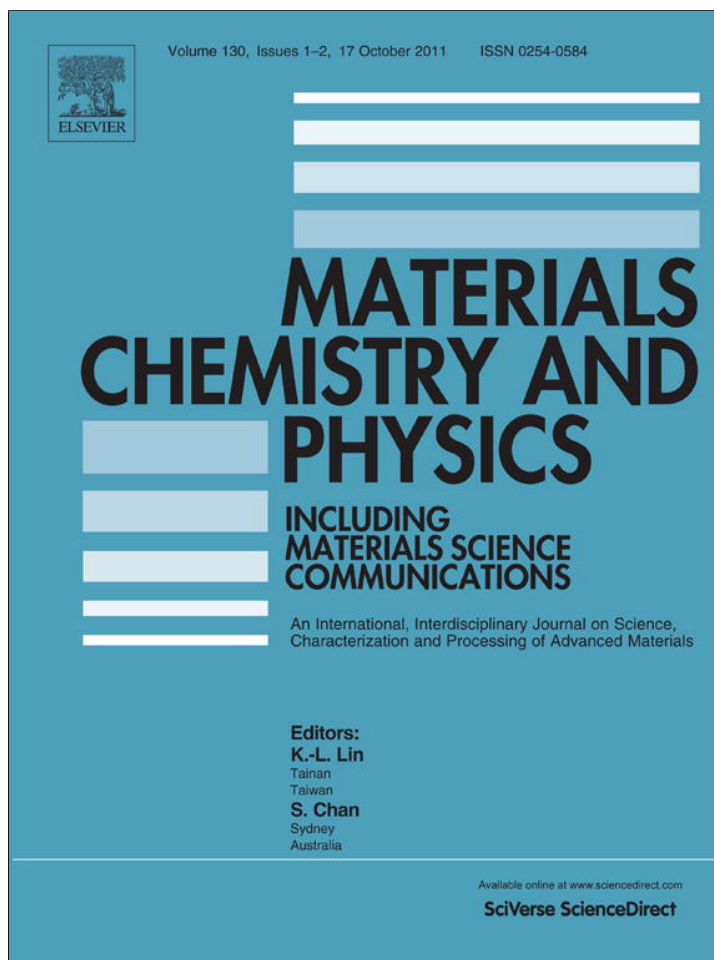


Provided for non-commercial research and education use.
Not for reproduction, distribution or commercial use.



This article appeared in a journal published by Elsevier. The attached copy is furnished to the author for internal non-commercial research and education use, including for instruction at the authors institution and sharing with colleagues.

Other uses, including reproduction and distribution, or selling or licensing copies, or posting to personal, institutional or third party websites are prohibited.

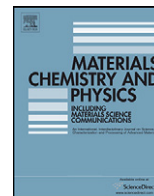
In most cases authors are permitted to post their version of the article (e.g. in Word or Tex form) to their personal website or institutional repository. Authors requiring further information regarding Elsevier's archiving and manuscript policies are encouraged to visit:

<http://www.elsevier.com/copyright>



Contents lists available at ScienceDirect

Materials Chemistry and Physics

journal homepage: www.elsevier.com/locate/matchemphys

Effect of templates on inverse opals fabricated through annular self-assembly/sol-gel method

Dengteng Ge^a, Lili Yang^b, Zeng Fan^a, Jiupeng Zhao^c, Yao Li^{a,*}^a Center for Composite Materials and Structures, Harbin Institute of Technology, P.O. Box 3010, No. 2 Yikuang Street, Harbin 150080, PR China^b School of Transportation Science and Engineering, Harbin Institute of Technology, Harbin 150090, PR China^c School of Chemical Engineering and Technology, Harbin Institute of Technology, Harbin 150001, PR China

ARTICLE INFO

Article history:

Received 26 November 2010

Received in revised form 19 February 2011

Accepted 7 May 2011

Keywords:

Sol-gel growth

Thin films

Small-angle scattering

ABSTRACT

There is a strong interest in simple preparation of flexible inverse opals for applications. In this article, indium tin oxides (ITO) flexible inverse opals were prepared through annular growth of templates and sol-gel process. It is shown that this method provides a facile route for large scale flexible inverse opals with excellent ordered structures. ITO materials are found much denser in inverse opals, which is due to the increased capillary force during drying process and enhanced shrinkage during annealing process. It is also found that the crystalline grains are refined and the photoluminescence performance is strengthened in low frequency.

Crown Copyright © 2011 Published by Elsevier B.V. All rights reserved.

1. Introduction

Inverse opals, also known as three-dimensional ordered macroporous (3DOM) materials, have been of great interest owing to the simplicity, highly accessible surface areas and better tunable stop band [1]. A typical procedure for fabrication of inverse opals includes three steps, namely, self-assembly of opals, infiltration of desired materials and removal of templates. For large scale preparation of opals, several methods have been studied and used [2–6]. Combined self-assembly/sol-gel technique has obtained increasing interest due to its versatility, including the ease of fine tuning, low cost and no requirement on substrates' conductivity, hardness or smoothness [3]. Various oxides, for example, TiO₂, SiO₂, Eu₂O₃ and Li_{0.35}La_{0.55}TiO₃ have been formed into inverse opals through this method [7–9]. However, seldom study on the preparation of inverse opals on flexible substrates through this method has been reported. Just Fortes et al. [10] prepared inverse opals on polyimide (PI) substrates. Moreover, previous research focused on the effect of sol-gel process on the microstructure of infiltrated materials or ordered macroporous structures, such as the infiltration repeating times, concentration of solutions or calcination temperature, etc. While the effect of the template has been always neglected. In this paper, annular growth of templates was firstly proposed for simple fabrication of templates on flexible substrates and the effect of templates on the microstructure of infiltrated materials

were also studied. As a semiconducting material, indium tin oxide (ITO) is chosen due to its excellent optical and photoelectric performance and wide applications in solar cells as antireflective layer, energy-efficient glazing as infrared reflective coating, and liquid crystal display [11–13] etc. To investigate the nanostructure of ITO infiltrated materials, small angle X-ray scattering (SAXS) technique was introduced. To the best of our knowledge, SAXS technique is the most accurate and non-destructive method for the structural characterization of particle systems [14].

2. Experimental

2.1. Annular growth of PS latex templates

Monodispersed polystyrene (PS) microspheres with relative standard deviation smaller than 4% (on the diameter) were obtained by an emulsifier-free emulsion polymerization technique [15]. As flexible substrates, PI films were cut into rectangle of 60 mm × 30 mm and then curly stick to the inner surfaces of cylindrical vessels for PS template growth. In that case PI substrates could keep their flexibility and the largest contact area with the dispersion. PS dispersion with a concentration of 0.1% was added into the vessels and dried in an incubator at a stable temperature and humidity. After water slowly evaporated, well ordered PS opals can be formed on the substrates.

2.2. Sol-gel fabrication of ITO inverse opals and ITO thin films

Hydrated indium nitrate (In(NO₃)₃·4.5H₂O) was dissolved in acetylacetone (AcAc) and then kept in an oven for 2 h at 83 °C. Hydrate tin tetrachloride (SnCl₄·5H₂O) was added to isopropanol. Two solutions were mixed to give the In/Sn atomic ratio of 9:1 and the concentration of 0.1 mol L⁻¹. The color of solutions turned optically from light yellow to orange-yellow, which implied the formation of In₂O₃ nanoparticles with an initial incorporation of Sn dopant atoms [16].

Dip-coating process at a constant withdrawal rate of 1 cm min⁻¹ was performed twice to guarantee the ITO precursor full infiltrated into the PS templates. The

* Corresponding author.

E-mail address: liyao@hit.edu.cn (Y. Li).

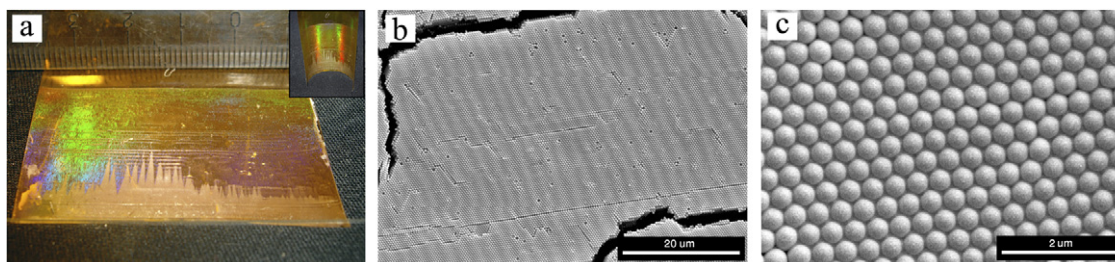


Fig. 1. (a) A piece of PS colloidal crystal sample. (b) Low magnification SEM image of PS colloidal crystal and (c) high magnification SEM of PS template showing close-packed spheres.

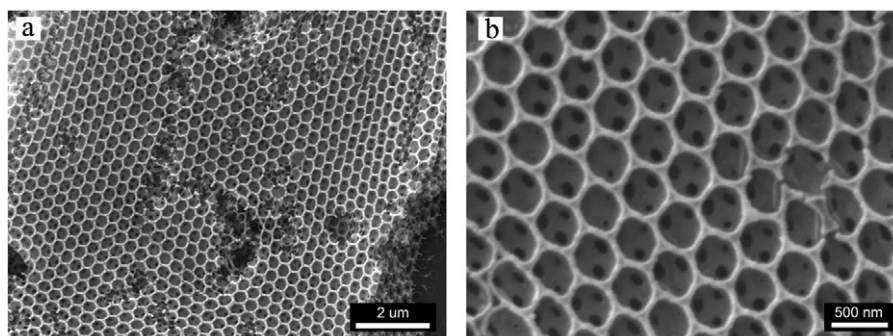


Fig. 2. (a) Low magnification SEM image of 3DOM ITO showing close-packed macropores, which are interconnected through window. (b) High magnification SEM of 3DOM ITO. The white regions are walls of the first layer, the gray regions are walls of the second layer, and the black regions are voids.

composites were subsequently dried for 24 h. Following calcinations in air at 200 °C (ramp of 1 °C min⁻¹) for 2 h and 350 °C (ramp of 10 °C min⁻¹) for 2 h were performed. ITO thin films on PI substrates without templates were also prepared through the same process.

2.3. Characterization

Scanning electronic microscopy (SEM) was performed by a QUANTA 200F (FEI, America). A Hitachi H-7650 transmission electronic microscopy (TEM) was used to study structures of ITO materials. Before the TEM tests, ITO thin films were carefully scraped onto the copper nets. X-ray diffraction (XRD) measurements were conducted using monochromatic Cu-K_α radiation with D/MAX2200 diffractometer (Rigaku, Japan). The photoluminescence property was tested by Cary Eclipse fluorescence spectrophotometer. SAXS experiments were performed at Shanghai Synchrotron Radiation Facility (SSRF) on the BL16B1 beamline using wavelength of 0.155 nm. A distance of 1.7 m between the sample and the detector was operated, at which length scales between 1.5 nm and 150 nm are resolvable.

3. Results and discussion

3.1. Annular growth of templates

Fig. 1a shows the PS template with a size of 45 mm × 30 mm. It is indicated that a large area of PS template was deposited on

the flexible PI substrates uniformly and easily. Significant colors were observed by naked-eyes. SEM image in Fig. 1b shows the area of ordered structures of template between two adjacent cracks is about 60 μm × 40 μm. However, a few defects and regular cracks could be still observed. From Fig. 1c, the center-to-center distance of PS sphere D is obtained 410 nm through direct measurement. The ordered structure prepared by annular growth method was proved to be excellent and templates can be used for the fabrication of inverse opals.

3.2. Macroporous structure of ITO inverse opals

The 3DOM structure of ITO inverse opals belongs to the shell structure (ShS) from Fig. 2. This is related with the solvent evaporation during the sol-gel process. When the gel formation is connected with much solvent evaporation, it results in a large shrinkage. The gel covers the inner surface of the opal only, leading to shell systems [3]. A long-range ordered macroporous network remains after the dissolution of solvent. These views not only reveal the excellent uniformity of structural details such as wall thickness and interconnecting windows, but also underline the efficiency of

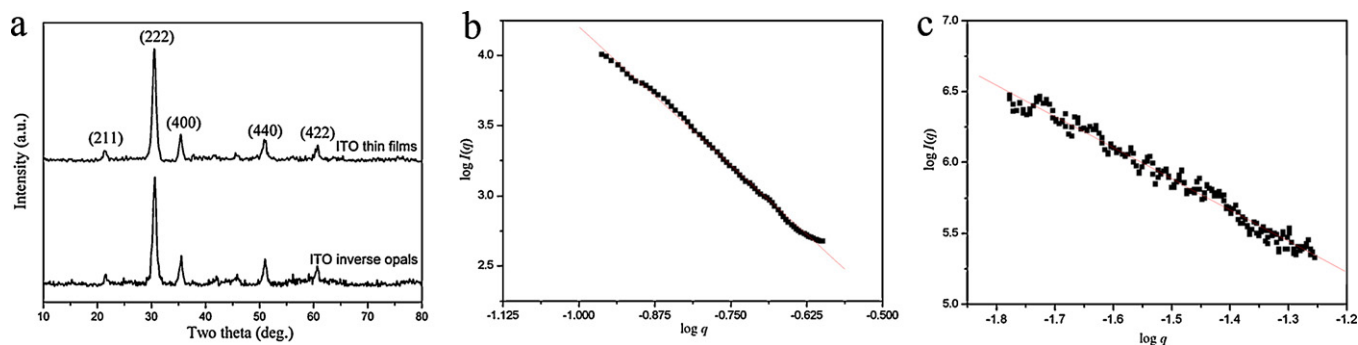


Fig. 3. (a) XRD patterns of ITO inverse opals and ITO thin films. (b) $\log I(q)$ vs. $\log q$ curve of ITO macroporous films' SAXS image (c) $\log I(q)$ vs. $\log q$ curve of ITO films' SAXS image.

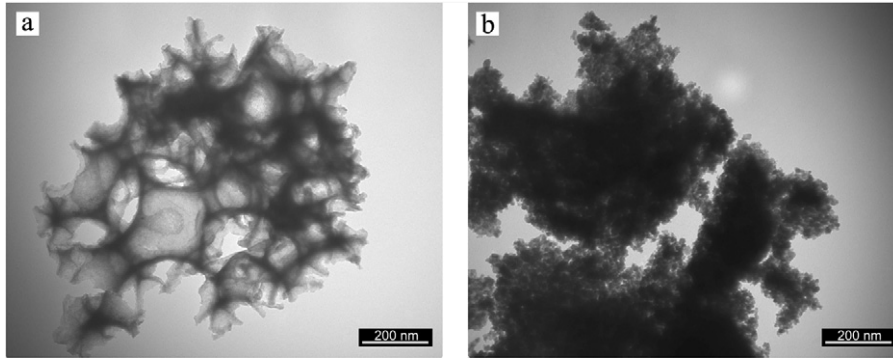


Fig. 4. (a) TEM image of ITO inverse opals and (b) ITO thin films.

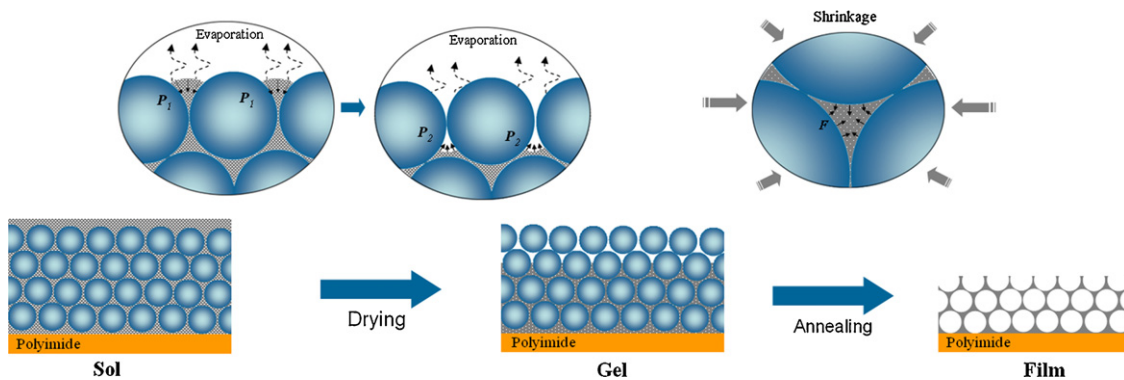


Fig. 5. Schematic plot of densification process during the formation of ITO inverse opals.

the infiltration process. Moreover, the center-to-center distance of macropores D is estimated 370 nm through direct measurement. It is demonstrated that the annealing process can keep the ordered structures but gives a shrinkage up to 10%. This is attributed to the shrinkage of infiltrated ITO materials due to the pore elimination during the annealing process.

3.3. Microstructure of infiltrated materials

The microstructures of infiltrated materials were investigated by XRD, SAXS and TEM techniques. Fig. 3a shows the XRD patterns of ITO inverse opals and ITO thin films to determine their crystalline structures. They are consistent with each other, proving that there is no preferred orientation of crystalline growth with the addition of ordered structures. The crystalline grain size was estimated from the width of the (2 2 2) diffraction peak at half maximum using the Scherrer equation. The crystalline sizes of ITO with

and without templates are estimated about 5 nm and 7 nm. It is suggested that crystalline growth is limited with the templates to some extent, which could be explained by the spatial confined effect of macroporous structure.

To give further information about the aggregation of particles/clusters, Fig. 3b shows the $\log I(q)$ vs. $\log q$ curve of inverse opals' SAXS results. The scattering intensity has a power-law with scattering vector shown as $I(q) = Cq^{-\alpha}$ [16]. Through linear fit, the value of α is obtained 3.9, which indicates a diffuse interface structure of ITO materials, i.e. a continuous electron-density change across the boundary [17]. The Schmidt exponent β was introduced to describe the concentration decay of the diffuse interface and it can be calculated from:

$$I(q) = Cq^{-3-2\beta} \quad (1)$$

Thus the Schmidt exponent of inverse opals $\beta_{IO} = 0.45$ is obtained. This value is very close to that of perfect dense material ($\beta = 0.5$).

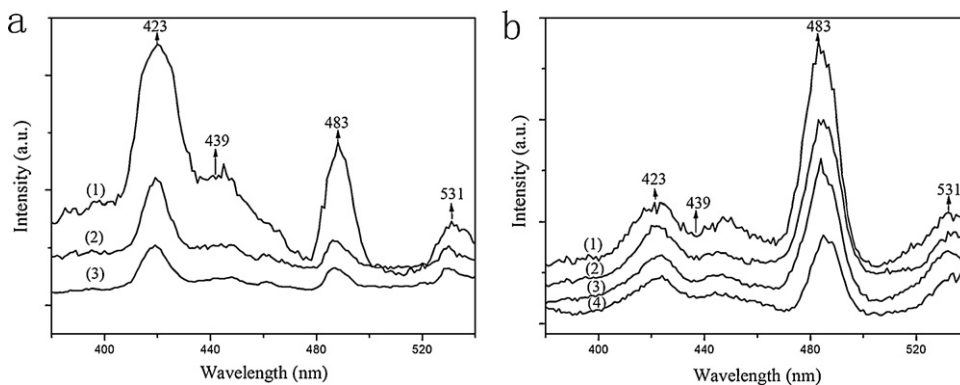


Fig. 6. (a) ITO films excited at: (1) 260 (2) 250 nm (3) 240 nm and (b) ITO inverse opals at (1) 240 nm; (2) 250 nm; (3) 260 nm; (4) 270 nm.

Thus ITO materials infiltrated into spheres were essentially compact with porosity at the edge.

Fig. 3c shows ITO thin films' $\log I(q)$ vs. $\log q$ curve of their SAXS results. The exponent parameter α is obtained 2.6, which represents a mass fractal structure of ITO materials. For mass fractal structures, the Porod's law is described as:

$$I(q) = Cq^{-D_m} \quad (2)$$

The mass fractal dimension of ITO films $D_m = 2.6$ is obtained, which is smaller than that of perfect dense materials ($D_m = 3$). It is obvious that a more compact network of the infiltrated ITO materials through sol-gel method is obtained due to the existing of templates.

The microstructures of ITO films with and without templates are also characterized by TEM technique, seen in Fig. 4. A typical ordered macroporous structure with a center-to-center distance D of 375 nm was shown. It is obvious that relatively denser structure is observed in inverse opals. TEM results also prove that the templates have influences on the microstructure of infiltrated materials.

As well known, the shrinkage of sol-gel materials is driven by minimization of the surface tension through the capillary pressure during the processes of drying and thermal treatments. Fig. 5 shows the schematic of drying and annealing processes of ITO inverse opals. The curvature of the menisci causes the liquid to be in tension and the network in compression. Generally the magnitude of capillary pressure P_c is estimated by the Laplace equation [18]:

$$P_c = \frac{-2\gamma_{LV} \cos(\theta)}{r_p} \quad (3)$$

where γ_{LV} is the surface tension between liquid and gas, θ is the wetting angle and r_p is the radius of meniscus curvature. For wetting pore fluids, P_c could be large and the capillary pressure thus represents a strong driving force to densify the deposited film. It is obvious that r_p in ITO inverse opals is much smaller than that in ITO thin films. Thus the capillary pressure P_c would be greatly increased, which results in further shrinkage of infiltrated ITO materials during the evaporation of solvent. Secondly, the surface area of ITO inverse opals is larger than that of ITO thin films due to the macroporous structure. During the annealing process, the shrinkage of substrates leads to a greater densification of ITO network through the internal forces from the interfaces.

3.4. Photoluminescence performance

The photoluminescence (PL) spectra of ITO films and inverse opals are shown in Fig. 6. It is obvious that three PL bands appeared at 423, 483 and 531 nm with a shoulder at 439 nm in both spectra. It is already believed by other workers that emissions for both bound and free excitons would appear when the PL excitation wavelength λ_{ex} is equivalent to position of bandgap λ_g and emissions for only free excitons in the case λ_{ex} is $>\lambda_g$ or $<\lambda_g$. We excited the samples at 240–270 nm in the PL tests, so these PL peaks are due to the free excitons [19–21]. Furthermore, the difference between these two curves is the position of PL band with strongest excitation intensity. The variation of excitation is attributed to the change

of nanocluster size [22]. It is suggested that the refinement of particles/clusters increases the excitation energy in the large wave band.

4. Conclusions

A novel simple fabrication of flexible inverse opals through annular growth/sol-gel method and the effect of templates were represented in this work. It is shown that the templates have excellent ordered structures through annular growth self-assembly method. An enhanced densification of ITO network is due to the existence of templates during the drying and annealing process. Moreover, a spatial confined effect due to the existence of ordered templates not only limits the crystalline growth but also improves the photoluminescence performance.

Acknowledgements

The authors wish to acknowledge Prof. Zhonghua Wu and his team for help in SAXS experiments from BSRF, Beijing, China. We also thank Prof. Jianhua He and Ph.D. Zhijun Li for carrying out SAXS tests at SSRF, Shanghai, China. This work is supported by the Program for New Century Excellent Talents (NCET-08-0168), National Natural Science Foundation (20601006), National Postdoctoral Foundation (20100471033) and the Fundamental Research Funds for the Central Universities (Grant No. HIT.ICRST.2010001 & HIT.NSRIF.2010034).

References

- [1] J.E.G.J. Wijnhoven, W.L. Vos, *Science* 28 (1998) 802.
- [2] J.D. Joannopoulos, R.D. Meade, J.N. Winn, *Photonic Crystals: Molding The Flow of Light*, Princeton University Press, 1995, p. 3.
- [3] F. Marlow, D. Konjhodzic, H. Bretinger, H.L. Li, *Adv. Sol. State Phys.* 45 (2005) 149–161.
- [4] A. Blanco, E. Chomski, S. Grabtchak, M. Ibsate, J. Sajeev, S.W. Leonard, C. Lopez, F. Meseguer, H. Miguez, J.P. Mondia, G.A. Ozin, O. Toader, H.M. Van Driel, *Nature* 405 (2000) 437.
- [5] X.D. Yu, Y.J. Lee, R. Furstenberg, J.O. White, P.V. Braun, *Adv. Mater.* 19 (2007) 1689–1692.
- [6] J.S. King, C.W. Neff, C.J. Summers, W. Park, S. Blomquist, E. Forsythe, D. Morton, *Appl. Phys. Lett.* 83 (2003) 2566.
- [7] M.C. Goncalves, J. Bras, R.M. Almeida, *J. Sol-gel Sci. Technol.* 42 (2007) 135–143.
- [8] Y.G. Zhang, Z.B. Lei, J.M. Li, S. Lu, *New J. Chem.* 25 (2001) 1118–1120.
- [9] M. Hara, H. Nakano, K. Dokko, S. Okuda, A. Kaeriyama, K. Kanamura, *J. Power Sources* 189 (2009) 485–489.
- [10] L.M. Fortes, M.C. Goncalves, R.M. Almeida, *Opt. Mater.* 33 (2011) 408.
- [11] J.D. Joannopoulos, P.R. Villeneuve, S. Fan, *Nature* 386 (1997) 143.
- [12] L.L. Yang, D.T. Ge, X.D. He, F. He, Y.B. Li, S. Zhang, *Thin Solid Films* 517 (2009) 5151–5156.
- [13] K.P. Musselman, G.J. Mulholland, A.P. Robinson, L.S. Mende, J.L.M. Driscoll, *Adv. Mater.* 20 (23) (2008) 4470–4475.
- [14] M. Birkholz, *Thin Film Analysis by X-ray Scattering*, Wiley-VCH, 2006, p3.
- [15] M.A. McLachlan, N.P. Johnson, R.M. Rue La De, D.W. McComb, *J. Mater. Chem.* 14 (2004) 144–150.
- [16] Z.Y. Sun, J.B. He, A. Kumbhar, J. Fang, *Langmuir* 26 (6) (2010) 4246.
- [17] Po-zen Wong, *Phys. Rev. B* 32 (1985) 7417.
- [18] P.W. Schmidt, D. Avnir, D. Levy, A. Hohn, M. Steiner, A. Roll, *J. Chem. Phys.* 94 (2) (1991) 1474.
- [19] C.J. Brinker, A.J. Hurd, *J. Phys.* 4 (1994) 1237.
- [20] K. Nanda, S.N. Sahu, *Adv. Mater.* 13 (2001) 280.
- [21] S. Kundu, P.K. Biawas, *Chem. Phys. Lett.* 414 (2005) 109.
- [22] Q. Chen, X.J. Li, Y.B. Jia, J.S. Zhu, Z. Yuheng, *J. Phys. Condens. Matter.* 9 (1997) L151.